Surface relaxation and surface dynamics of $YBa_2Cu_3O_{7-\delta}$(001) slabs

1996 J. Phys.: Condens. Matter 8 10195

(http://iopscience.iop.org/0953-8984/8/49/011)

J. Phys.: Condens. Matter **8** (1996) 10195–10207. Printed in the UK

Surface relaxation and surface dynamics of $YBa_2Cu_3O_{7-\delta}$(001) slabs

L Philippe and Ph Lambin

Laboratoire de Physique du Solide, Département de Physique, Facultés Universitaires Notre-Dame de la Paix, rue de Bruxelles, 61 B-5000 Namur, Belgium

Received 12 July 1996, in final form 4 October 1996

Abstract. In the framework of a rigid-ion model, we analyse the dynamics of $YBa_2Cu_3O_{7-\delta}$ slabs. The cancellation of the total dipole moment of these slabs is assured by surface charge transfers which are estimated for different terminations. The corresponding surface geometric relaxations are calculated. We discuss and compare the dynamics of BaO terminated films on the basis of their dielectric surface function and the surface character of their phonons.

1. Introduction

Although many properties of high-temperature cuprate superconductors have been deeply investigated from both experiment and theory [1], very little is known about the surface dynamics of these compounds. It is only recently that helium atom scattering (HAS) experiments [2] and high-resolution electron-energy-loss spectroscopy (EELS) have brought some information about surface acoustical and optical phonons, respectively, of BiSCCO-2212 and YBCO-123 materials [3, 4]. The interpretation of these data by lattice dynamical calculations is made difficult by the complexity of the crystal. In this respect, surface lattice dynamics from *ab initio* calculations is out of reach of present computers, and remains questionable due to the failure of the LDA to correctly reproduce the band structure of most of the HTSC materials. On the other hand, fitting force constants to the measured bulk phonons of the HTSCs is a formidable task due to the large number of parameters involved, and this would probably lead to many different acceptable solutions having little chance of being applicable to a surface geometry. A shell model description of the dynamics allows one to reduce the number of parameters to a more reasonable set and, in principle, makes it possible to relax the surface energy according to the potential model used [5, 6]. However, relaxing HTSCs' surfaces is not simple, as these compounds are lamellar systems built from charged sub-molecular layers, and their bulk unit cells carry a net dipole moment, in noticable contrast with simple perovskites such as $SrTiO_3$ [7].

For all these reasons, we decided to investigate the surface dynamics of $YBa_2Cu_3O_{7-\delta}$ from the most simple description of the crystal, which we viewed as an ionic compound [8]. The rigid-ion model adopted for this work [9, 10] ignores the metallic character of the CuO_2 sheets, which could partly be accounted for in the bulk with a suitable screening of the Coulomb interactions [11], but this could hardly be adapted to the surface problem. The dynamical model also ignores the local electronic polarizabilities [6] and is based on very few adjustable parameters. It has the advantage, over many other models we have examined, of working for (001) surfaces of $YBa_2Cu_3O_{7-\delta}$ without changes of the parameters other than

0953-8984/96/4910195+13$19.50

the ones involved in the energy relaxation. With this model at hand, we determined the phonon band structure of ideal (001) films of the $\delta = 0$ and $\delta = 1$ compounds. We computed the surface characters of the modes throughout the two-dimensional first Brillouin zone in order to identify those phonons that are localized at the surface. In addition, the surface dielectric response function of the phonons was determined close to the zone centre. Within the validity limits of the model, the present calculations confirm that long-wavelength surface optical phonons of the cuprate superconductors can be excited in EELS experiments and that the actual termination of the crystal at the surface has little influence on the EELS spectra. The loss intensities predicted for $YBa_2Cu_3O_7$ by the rigid-ion model are much larger than the ones measured experimentally, but this is due to the screening induced by the CuO_2 sheets [12].

The paper is organized as follows. In section 2, we present the lattice dynamics and the charge transfer models on which our investigations are based. We apply these models to the static case in order to determine the different surface relaxation patterns, systematically presented in section 3. In the next section, we analyse the dynamics of a pair of these relaxed surfaces and, finally, we give some conclusions in section 5.

2. Foundations

2.1. Dynamics model

In this study, we use a rigid-ion model constructed by Chaplot [9] where the total energy of the crystal is described as a sum of two-body potential interactions

$$V_{ij} = \frac{e^2}{4\pi\varepsilon_0}\frac{Q_i Q_j}{r_{ij}} + a\,\exp\left(-\frac{br_{ij}}{R_i + R_j}\right) - \frac{w}{r_{ij}^6} + cD\,\exp\left(-n\left(r_{ij} - r_0\right)^2/2cr_{ij}\right). \qquad (1)$$

The first term corresponds to the coulombic potential interaction between point ions i and j. It depends on the distance between these two ions, r_{ij}, and on their charges, Q_i and Q_j. The next term is an effective repulsive potential in the usual Born–Mayer form with an exponential range calculated as the sum of ionic radii, R_i and R_j, divided by a scaling constant b. The third term simulates van der Waals attraction between oxygen atoms. Finally, the fourth term is a Lippincott–Schroeder 'covalent' potential which is only set between copper and oxygen atoms situated in CuO_2 planes or $CuO_{1-\delta}$ chains. This last term stabilizes Cu–O interactions for a distance r_0 fixed to 0.18 nm. The other parameters are $e^2/(4\pi\varepsilon_0) = 1.44$ eV nm, $a = 1822$ eV, $b = 12.364$, $w = 50 \times 10^{-6}$ eV nm^6, $c = 0.5$, $D = 1$ eV, $n = 80$ nm^{-1}. All the ionic parameters are listed in table 1. For completeness, the crystallographic parameters are summarized in table 2 for the structures which correspond to minima of the total potential energy with respect to degrees of freedom compatible with crystallographic symmetry ($Pmmm$ and $P4/mmm$ for $YBa_2Cu_3O_7$ and $YBa_2Cu_3O_6$, respectively).

2.2. Charge transfers

In the framework of rigid-ion models applied to slab geometry, we have to take into account the presence of a residual dipole moment associated with an extensive excess of energy with respect to bulk material [13]. As proposed by Prade *et al* [7] for a cubic perovskite such as $SrTiO_3$, we could tackle this problem by imposing neutrality to sub-molecular layers. For high-T_c materials, however, this method has to be rejected since charge transfers do exist between conductor planes (CuO_2) and charge reservoir (e.g.Y–BaO–$CuO_{1-\delta}$). Another

Table 1. Effective charge, Z, and ionic radii, R, used in the rigid-ion model of $YBa_2Cu_3O_{7-\delta}$. Cu(1) refers to copper atoms of CuO chains whereas Cu(2) concerns copper atoms of CuO_2 planes.

	$\delta = 0$		$\delta = 1$	
Atom	Z (e)	R (nm)	Z (e)	R (nm)
Y	1.9	0.178	1.9	0.178
Ba	1.5	0.230	1.25	0.210
Cu(1)	1.4	0.120	0.6	0.110
Cu(2)	1.4	0.120	1.4	0.120
O	−1.3	0.174	−1.3	0.174

Table 2. Crystallographic parameters of the minimal-potential-energy structures for the two extreme compounds of the $YBa_2Cu_3O_{7-\delta}$ family. Fractional coordinates are Y (0.5,0.5,0.5), Ba (0.5,0.5,z_1), Cu(1) (0,0,0), Cu(2) (0,0,z_2),O(1) (0,0,z_3), O(2) (0.5,0,z_4), O(3) (0,0.5,z_5) and O(4) (0,0.5,0). For $YBa_2Cu_3O_6$, oxygen atoms of the CuO_2 planes are equivalent ($z_4 = z_5$) (bracketed figures refers to experimental data [22]).

	$\delta = 0$	$\delta = 1$
a (nm)	0.380 (0.381)	0.376 (0.383)
b (nm)	0.382 (0.387)	0.376 (0.383)
c (nm)	1.169 (1.163)	1.176 (1.174)
z_1	0.189 (0.184)	0.204 (0.194)
z_2	0.352 (0.355)	0.350 (0.361)
z_3	0.162 (0.158)	0.160 (0.153)
z_4	0.380 (0.378)	0.380 (0.379)
z_5	0.380 (0.377)	0.380 (0.379)

natural way to solve this problem consists in considering non-stoichiometric but symmetric slabs [14]. In this case, the presence of non-neutral sub-molecular layers implies charge exchanges with the external world to assure the global neutrality condition. In all cases, the question we have to address now is to determine the microscopic distribution of macroscopic charge transfers [15].

In the following, we will use the notations introduced by Streitz and Mintmire [16]. In this approach, the total potential energy of an array of atoms is described as a function of atomic charges, Q_i, and positions, r_i, of the form

$$E_{es}\left(\{r_{ij}\}\{Q_i\}\right) = \frac{1}{2}\sum_{i,j=1}^{N} V_{LR\,ij}\left(r_{ij}\right) Q_i Q_j + \sum_{i=1}^{N} E_i\left(Q_i\right) + \frac{1}{2}\sum_{i,j=1}^{N} V_{SR\,ij}\left(r_{ij}\right) \tag{2}$$

where N is the number of sites per unit cell, $V_{LR\,ij}$ is the inverse electrostatic induction coefficient for sites i and j [17], E_i is the on-site electronic energy and $V_{SR\,ij}$ corresponds to short-range interactions. At this point, the cell neutrality permits us to normalize the diagonal coefficients of the long-range part, $V_{LR\,ii}$, to zero. The first and third terms in equation (2) depend on the atomic positions and are treated by lattice dynamics. Here, we shall first consider the modification of ionic internal energy (first and second terms in equation (2)) caused by charge transfers in a geometrically invariant structure.

For bulk material, we can expand $E_i(Q_i)$ in a Taylor series in terms of the variations

of the charges with respect to their bulk values. We thus obtain

$$E_{es} = \frac{1}{2}\sum_{ij=1}^{N} V^b_{LR\,ij}\,Q_i\,Q_j + \sum_{i=1}^{N}\left[E_{i0} + \chi_i\,\Delta Q_i + \frac{1}{2}\eta_i\,(\Delta Q_i)^2 + \cdots\right] \tag{3}$$

where we introduce the electronegativity, χ_i, and the ionic hardness, η_i, defined at bulk charge values, Q_i^b [18]. This set of values corresponds to a minimum of the total potential energy in the parameter space defined by the neutrality condition

$$\sum_{i=1}^{N} Q_i = 0. \tag{4}$$

This will be the case if the following relation is verified for each atom i:

$$\sum_{j=1}^{N} V^b_{LR\,ij}\,Q_j^b + \chi_i = \mu^b \tag{5}$$

where μ^b is the Lagrange multiplier associated with the constraint (4). At equilibrium, μ^b is a common quantity for all the atoms, defined as the *chemical potential* of the bulk material. In the following, μ^b will be considered as a reference level that we decide to equal to zero. In this case, electronegativities are simply equal to the opposite of the Madelung potentials, independently of hardnesses. At this point, the role of these parameters is limited to assuring the positiveness of the quadratic form (3) so that its extremum is a minimum.

We turn now to slab geometry. Let us assume that, due to the presence of macroscopic electric field, only the inverse influence coefficients are modified. Therefore, the new quadratic form can be written as

$$E_{es} = \frac{1}{2}\sum_{ij=1}^{N} V^s_{ij}\,Q_i\,Q_j + \sum_{i=1}^{N}\left[E_{i0} - \left(\sum_{i=1}^{N} V^b_{LR\,ij}\,Q_j^b\right)\Delta Q_i + \frac{1}{2}\eta_i\,(\Delta Q_i)^2 + \cdots\right] \tag{6}$$

where we have replaced the bulk electronegativity by its value deduced from (5). If we limit this expansion to the second order, we obtain

$$E_{es} = E_{0es} + \frac{1}{2}\sum_{ij=1}^{N} A_{ij}\,Q_i\,Q_j + \sum_{i=1}^{N} B_i\,Q_i \tag{7}$$

with $A_{ij} = V^s_{ij} + \delta_{ij}\eta_i$ and $B_i = -\sum_{j=1}^{N} V^b_{ij}Q_j^b - \eta_i Q_i^b$.

In the parameter space defined by the neutrality constraint (equation (4)), we determine the new minimum defined now by the N following conditions

$$\sum_{j=1}^{N} A_{ij}q_j^s + B_i = \mu^s. \tag{8}$$

From these relations, we deduce the slab charge, Q_i^s, and the slab chemical potential, μ^s, as

$$Q_i^s = \sum_{j=1}^{N} A_{ij}^{-1}\left(\mu^s - B_i\right) \tag{9}$$

$$\mu^s = \frac{\sum_{ij=1}^{N} A_{ij}^{-1}B_i}{\sum_{ij=1}^{N} A_{ij}^{-1}}. \tag{10}$$

We note that these surface quantities depend on the ionic hardnesses, which constitute the sole parameters not contained in the rigid-ion model.

In summary, we claim that we can calculate surface charge on the basis of bulk charge, structure and hardness deduced from the ionization curve at the same charge value (table 3). For oxygen, this value was set to 6.0 as a minimum to guarantee the positiveness of the matrix.

Table 3. Ionic hardness parameters η for the two extremal compounds of the $YBa_2Cu_3O_{7-\delta}$ family.

	η (V e^{-1})	
Atom	$\delta = 0$	$\delta = 1$
Y	4.0	4.0
Ba	7.6	5.0
Cu(1)	7.1	5.5
Cu(2)	7.1	7.1
O	6.0	6.0

3. Surface relaxations

3.1. Description of the different terminations

The structure of $YBa_2Cu_3O_{7-\delta}$ can be described as a lamellar material composed of six layers per unit cell: $CuO_{1-\delta}$, BaO, CuO_2, Y, CuO_2 and BaO (figure 1). Let us notice that these layers are not perfectly planar. For example, the z-extension of the BaO and CuO_2 layers is of the order of 0.03 nm. If we restrict our investigation to stoichiometric slabs, we can only construct three types of film [19]: (a) $CuO_{1-\delta}$–BaO$\cdots$$CuO_2$–BaO; (b) CuO_2–Y$\cdots$$CuO_{1-\delta}$–BaO; (c) Y–$CuO_2\cdots$BaO–$CuO_2$. In the following, we shall not consider slabs of the third kind because of their extremely polar yttrium surface which cannot be stabilized with the present relaxation scheme.

3.2. Charge and geometric relaxations

Firstly, we note that charge optimization implies a quasi-perfect cancellation of the dipole moment of the slab (table 4). After relaxation, this quantity ceases to be an extensive property so the excess energy per unit cell tends to zero with increasing slab thickness. Moreover, we note that this cancellation is always compatible with decreasing the absolute charges of all the ions (tables 5–8), even if the total charge carried by an atomic layer may increase (see, for example, the charge of the BaO surface layer for the CuO–BaO$\cdots$$CuO_2$–BaO film which increases from $+0.20$ e (table 9) to $+0.28$ e (table 5)). Finally, the low anisotropy of $YBa_2Cu_3O_7$ at the static level is confirmed here by a common behaviour for the two oxygen atoms of the CuO_2 layers.

In $YBa_2Cu_3O_6$, stoichiometric modifications with respect to the $YBa_2Cu_3O_7$ compound imply the presence of pure copper layers ($+0.6$ e). These charge modifications of $CuO_{1-\delta}$ layers are compensated by charge transfer with the next BaO planes. Interestingly $YBa_2Cu_3O_6$ and $YBa_2Cu_3O_7$ films of type (b) have the same dipole moment per unit cell (table 4), which the charge relaxation neutralizes by transferring the same amount (δQ = 0.25, see tables 6 and 8) from one face to the other in the two compounds. For slabs of type (a), the increase of the total dipolar moment on going from δ = 0 to δ = 1 is reflected in a larger charge transfer in the latter compound, which results in a quasi-neutral copper layer at the free surface (table 7).

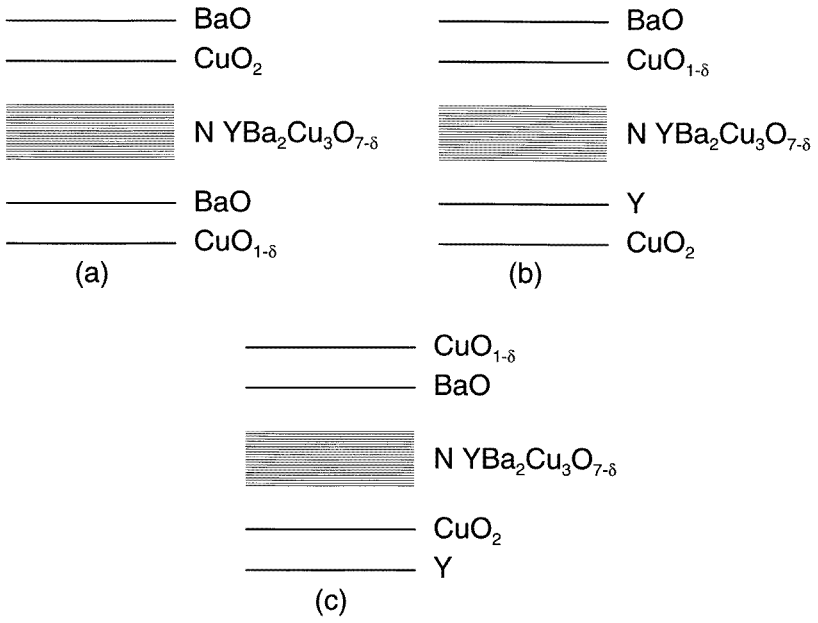

Figure 1. Sketch of the three possible stoichiometric films of $YBa_2Cu_3O_{7-\delta}$.

Table 4. Dipolar moment per unit cell before and after charge relaxation for the two extremal compounds of the $YBa_2Cu_3O_{7-\delta}$ family.

		P_z (e nm/unit cell)	
Stoichiometric	Surface layers	Before relaxation	After relaxation
$YBa_2Cu_3O_7$	CuO–BaO–...–CuO_2–BaO	0.058	0.015
	CuO_2–Y–...–CuO–BaO	0.29	0.041
$YBa_2Cu_3O_6$	Cu–BaO–...–CuO_2–BaO	0.35	0.021
	CuO_2–Y–...–Cu–BaO	0.29	0.040

As a second step, we now consider geometric relaxations (tables 5–8). As expected, the cancellation of the macroscopic electric field implies that these relaxations are localized on no more than three atomic surface layers on each face of the slab. Moreover, the amplitudes of these relaxations are of the same order as the ones obtained for other perovskites such as $SrTiO_3$ [7]. As with the charge transfers, we notice the very low anisotropy of $YBa_2Cu_3O_7$: the two oxygen atoms in the CuO_2 layers are nearly equivalent. If we compare the two extreme compounds, the geometric relaxations are very similar for the common atomic layers Y and CuO_2. For the other layers, the relaxation amplitudes can be significantly different between the two materials. For instance the barium in the extreme surface layer of the films of type (b) moves by 0.024 nm in $YBa_2Cu_3O_6$ but only by 0.005 nm and in the opposite direction for the case of $YBa_2Cu_3O_7$. In fact, we know that coordinate relaxations are very sensitive to short-range interactions which, in this case, are profoundly modified by the stoichiometric changes in the next $CuO_{1-\delta}$ layer.

Table 5. Charge modifications and z-relaxation amplitudes for the two surfaces of a CuO–BaO···CuO_2–BaO terminated $YBa_2Cu_3O_7$ slab (type a) containing four molecular layers (positive amplitudes correspond to relaxation towards the exterior of the slab).

Layer	Q (e)	δQ (e)	Atom	Q (e)	δQ (e)	δz (nm)
CuO	0.00	−0.10	Cu(1)	1.06	−0.34	−0.001
			O	−1.05	0.25	0.017
BaO	0.25	0.05	Ba	1.48	−0.02	0.003
			O	−1.23	0.07	−0.006
			3 unit cells			
CuO_2	−1.23	−0.03	Cu(2)	1.35	−0.05	−0.007
			O(2)	−1.29	0.01	−0.002
			O(3)	−1.29	0.01	−0.001
BaO	0.28	0.08	Ba	1.37	−0.13	0.008
			O	−1.08	0.22	0.005

Table 6. Same as in table 5 for a CuO_2–Y···CuO–BaO terminated $YBa_2Cu_3O_7$ slab (type b).

Layer	Q (e)	δQ (e)	Atom	Q (e)	δQ (e)	δz (nm)
CuO_2	−0.73	0.47	Cu(2)	1.12	−0.28	0.024
			O(2)	−0.92	0.38	0.012
			O(3)	−0.93	0.37	0.014
Y	1.68	−0.22	Y	1.68	−0.22	−0.005
			3 unit cells			
CuO	0.12	0.02	Cu(1)	1.40	0.00	0.000
			O	−1.28	0.02	−0.002
BaO	−0.07	−0.27	Ba	1.25	−0.25	−0.005
			O	−1.32	−0.02	0.001

Table 7. Same as in table 5 for a Cu–BaO···CuO_2–BaO terminated $YBa_2Cu_3O_6$ slab (type a).

Layer	Q (e)	δQ (e)	Atom	Q (e)	δQ (e)	δz (nm)
Cu	0.12	−0.48	Cu(1)	0.12	−0.48	−0.018
BaO	0.13	0.18	Ba	1.19	−0.06	0.008
			O	−1.06	0.24	−0.005
			3 unit cells			
CuO_2	−1.25	−0.05	Cu(2)	1.33	−0.07	−0.011
			O	−1.29	0.01	−0.003
BaO	0.30	0.35	Ba	1.23	−0.02	0.010
			O	−0.93	0.37	0.004

4. Dynamics of the relaxed surfaces

A central quantity in the interpretation of EELS experiments is the so-called surface dielectric function $g(Q, \omega)$, which represents the response of the system to an electric excitation having the form of a plane wave with frequency ω and wavevector Q parallel to the surface [20]. In figure 2, we have plotted the imaginary part of the BaO surface dielectric response function of a slab of type (a) composed of ten molecular layers. The full curve

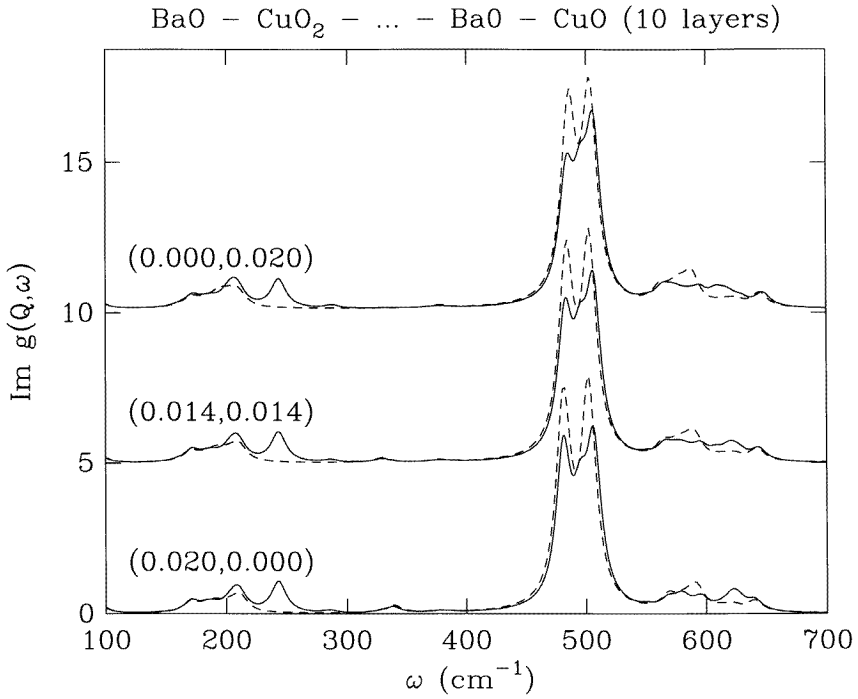

Figure 2. Imaginary part of the surface dielectric response function of a film of type (a) seen from its BaO termination and composed of ten molecular layers for three wavevectors of modulus 0.02 Å^{-1}. The full curves have been deduced from lattice dynamics calculation; the dashed curves result from electrostatics.

Table 8. Same as in table 5 for a CuO_2–Y···Cu–BaO terminated $YBa_2Cu_3O_6$ slab (type b).

Layer	Q (e)	δQ (e)	Atom	Q (e)	δQ (e)	δz (nm)
CuO_2	−0.72	0.48	Cu(2)	1.10	−0.30	0.027
			O	−0.91	0.39	0.014
Y	1.67	−0.23	Y	1.67	−0.23	−0.005
			3 unit cells			
Cu	0.60	0.00	Cu(1)	0.60	0.00	−0.001
BaO	−0.30	−0.25	Ba	0.71	−0.54	0.024
			O	−1.01	0.29	0.000

was obtained by lattice dynamics, whereas the dashed curve represents the result of the electrostatic theory [14] based on the dielectric function of the bulk material deduced from the same rigid-ion model. The dominant structure around 500 cm^{-1} in both determinations of Im[g] is due to a pair of Fuchs–Kliewer (FK) phonons. These surface macroscopic optical modes in turn dominate the EELS spectrum of the system. We call the reader's attention to a small peak around 260 cm^{-1} in the full curve which is due to a surface microscopic phonon with $SP_\perp$ polarization.

Figure 3 visualizes the surface character of the phonons of the same slab, reduced here to three molecular layers. This chart shows the dispersion curves of the phonons, with the

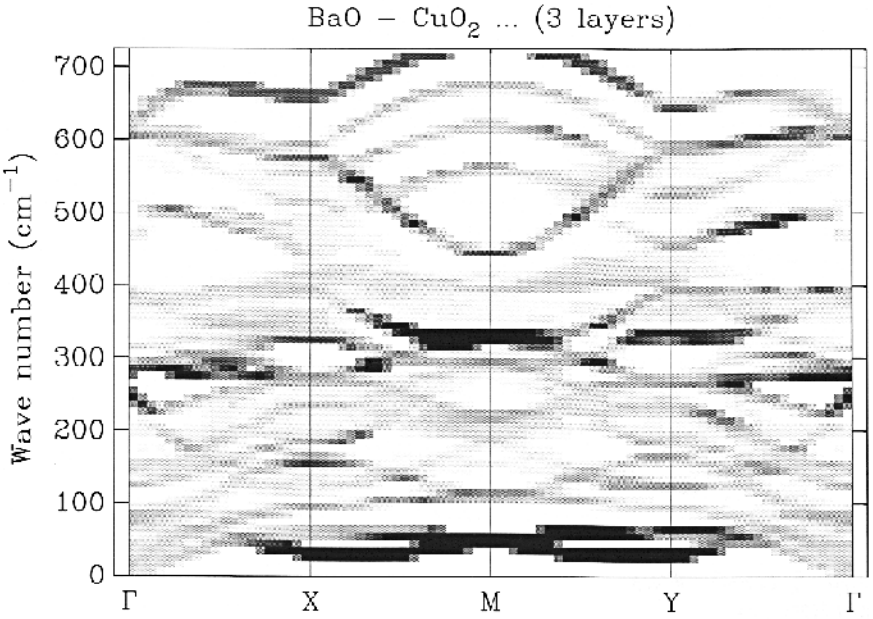

Figure 3. Dispersion curves of the phonons in a film of type (a) composed of three molecular layers. The grey scale depicts the BaO surface character of the modes (see text)

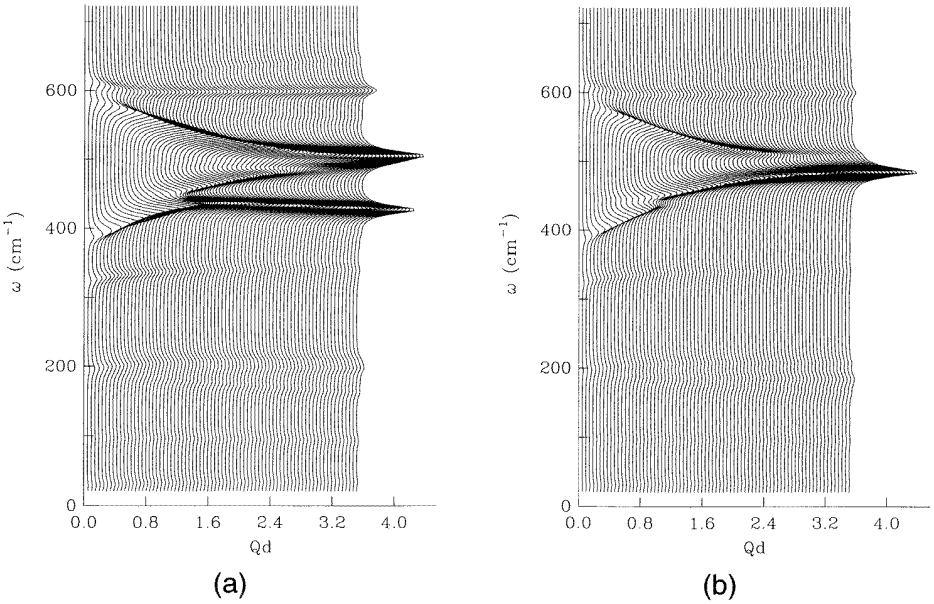

Figure 4. Imaginary part of the surface dielectric response function of a film of type (b) seen from, respectively, its CuO_2 (a) and BaO (b) terminations. The film is composed of ten molecular layers ($d = 11.6$ nm).

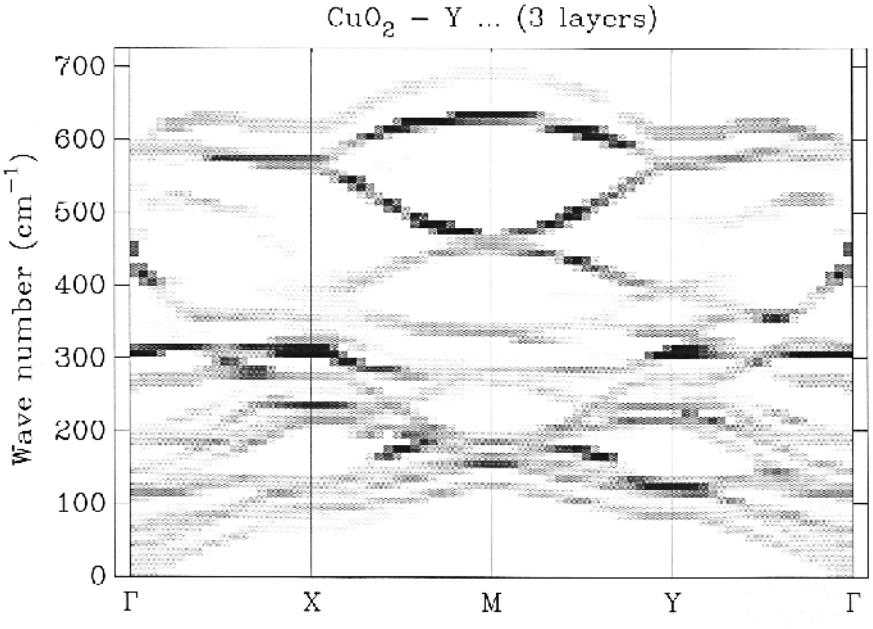

Figure 5. Same as in figure 3 for a film of type (b) seen from its CuO_2 side.

Table 9. Charge carried by atomic layers for the two extremal compounds of the $YBa_2Cu_3O_{7-\delta}$ family.

	Q_{layer} (e)	
Layer	$\delta = 0$	$\delta = 1$
$CuO_{1-\delta}$	0.1	0.6
BaO	0.2	−0.05
CuO_2	−1.2	−1.2
Y	1.9	1.9

grey scale representing the normalized vibrational squared amplitudes [21] summed over the atoms composing the BaO and CuO_2 topmost layers. At the Γ point, the branch at 260 cm^{-1} is the above-mentioned surface phonon. The structure near 285 cm^{-1} is a pair of surface phonons with polarization parallel to the surface and having little dielectric activity. Among the low-lying branches with high intensity (black) in the X–M–Y region, one is a Rayleigh phonon and the other involves vibrations of the heavy Ba ion only. In the domain of optical frequencies, the intense surface character at the M point for $\omega = 325$ cm^{-1} is due to a pair of phonons localized on the BaO and CuO_2 topmost layers with polarization parallel to the surface.

Considering now a slab of kind (b), figure 4 compares the imaginary parts of the surface dielectric response computed by lattice dynamics for the two surfaces (BaO on one end and CuO_2 on the other end). Most of the dielectric activity is concentrated again on a pair of FK phonons which disperse between 400 and 600 cm^{-1}. The peak at 600 cm^{-1} is another Fuchs–Kliewer phonon. The other, weaker structures are bulk modes already contained in the electrostatic theory, and which develop in frequency regions where the x or y principal

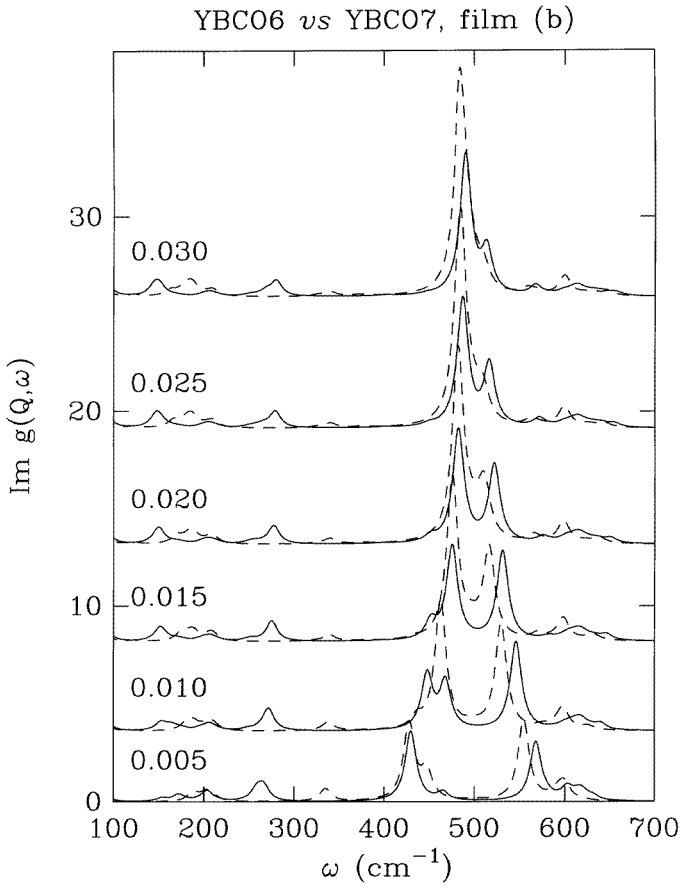

Figure 6. Imaginary part of the surface dielectric response function of films of type (b) made of $YBa_2Cu_3O_6$ (full curves) and $YBa_2Cu_3O_7$ (dashed curves) for wavevectors ranging from 0.005 to 0.030 $Å^{-1}$. The films, composed of ten molecular layers, are excited from their BaO sides.

components of the dielectric tensor have their signs opposite to the one of the z component.

We note that for the CuO_2 surface the low-frequency FK mode mixes and exchanges part of its character with a surface microscopic phonon at frequency 455 cm^{-1}. This mode is linearly polarized normal to the surface and concerns mostly the vibration of the O atoms of the topmost CuO_2 layer. The nearby Cu and Y atoms have weaker displacements in the opposite direction. This mode is visible in the character chart of figure 5 in the form of a branch with negative dispersion at the Γ point. In the same figure, the structure at 310 cm^{-1} is a pair of modes in which the Cu and one O vibrate against each other along the x and y directions, respectively. For the other termination, there is also a mixing of the low-frequency FK phonon with a surface microscopic phonon at 491 cm^{-1}. This again is polarized $SP_\perp$ and involves the vibration of the CuO chain immediately below the BaO surface layer.

In figure 6, the surface loss function Im $g(Q, \omega)$ of $YBa_2Cu_3O_6$ (full curves) is compared to that of $YBa_2Cu_3O_7$ (dashed curves) for increasing wavevectors Q. Films of type (b) composed of ten molecular layers have been considered in both cases, with the excitation

being applied from the BaO side. By reducing the amount of oxygen in the compound, there is a decrease of intensity of the modes between 400 and 600 cm^{-1}, and a blue shift of the high-frequency peaks. There is in particular the development of a structure above 600 cm^{-1} in the loss spectrum of $YBa_2Cu_3O_6$. This structure is due to both a Fuchs–Kliewer phonon and a continuum of bulk modes with a smaller intensity. By comparison $YBa_2Cu_3O_7$ has a Fuchs–Kliewer phonon at 600 cm^{-1}, as mentioned above. The fact that a loss peak was observed around 630 cm^{-1} in the experimental HREELS spectra of the YBCO superconductor has been taken as an indication that the composition at the surface is closer to $YBa_2Cu_3O_6$ than $YBa_2Cu_3O_7$ [4]. This argumentation seems reasonable in view of the present calculations, assuming that the EELS spectrum is dominated by the dipole scattering mechanism. It is not impossible however that non-infrared surface phonons with frequency above 600 cm^{-1} can be excited by inelastic impact scattering, which will make the identification of the surface layer less evident.

5. Conclusion

Surface relaxation of $YBa_2Cu_3O_{7-\delta}$ films has been made possible within a simple ionic picture and an energetic model which incorporates both geometrical and electrostatics degrees of freedom. Surface dynamics was successfully performed using this approach. The dynamical calculations revealed the existence of various surface microscopic phonons having a small dielectric activity near the Γ point. In this region, the optical surface macroscopic phonons dominate the surface dielectric response of $YBa_2Cu_3O_{7-\delta}$ films which were shown to be weakly dependent on the actual surface terminations. It is hoped that this model can be applied to other anisotropic purely ionic materials and metallic oxides.

Acknowledgments

This work was funded by the 'Incentive Program on High-Temperature Superconductivity' of the Belgian State. The authors acknowledge the use of Namur Scientific Computing Facility, a common project between the National Scientific Foundation, IBM Belgium and the Facultés Universitaires Notre-Dame de la Paix in Namur.

References

[1] For a review, refer to e.g. Plakida N M 1995 *High-Temperature Superconductivity, Experiment and Theory* (Berlin: Springer)
[2] Benedek G, Hofmann F and Ruggerone P 1994 *Surface Phonons in Layered Crystals: Theoretical Aspects* (Amsterdam: Elsevier)
[3] Phelps R B, Akavoor P, Kesmodel L, Barr A L, Markert J T, Ma J, Kelley R J and Onellion M 1994 *Phys. Rev.* B **50** 6526
[4] Franchy R, Decker B, Masuch J and Ibach H 1994 *Surf. Sci.* **303** 386
[5] Kress W, Schröder U, Prade J, Kulkarni A D and de Wette F W 1988 *Phys. Rev.* B **38** 2906
[6] Popov V N 1995 *J. Phys.: Condens. Matter* **7** 1625
[7] Prade J, Schröder U, Kress W, de Wette F W and Kulkarni A D 1993 *J. Phys.: Condens. Matter* **5** 1
[8] Torrance J B and Metzger R M 1989 *Phys. Rev. Lett.* **63** 1515
[9] Chaplot S L 1990 *Phys. Rev.* B **42** 2149
[10] Chaplot S L, Reichart W, Pintschovius L and Pyka N 1995 *Phys. Rev.* B **52** 7230
[11] Koval S, Migoni R and Bonadeo H 1992 *J. Phys.: Condens. Matter* **4** 4759
[12] Mills D L, Phelps R P and Kesmodel L L 1994 *Phys. Rev.* B **50** 6394
[13] Fripiat J G, Lucas A, André J-M and Derouane E G 1977 *Chem. Phys.* **21** 101
[14] Philippe L, Lambin Ph, Senet P and Lucas A A 1994 *Appl. Supercond.* **1** 135

[15] Philippe L 1995 *PhD Thesis* Facultés Universitaires Notre-Dame de la Paix
[16] Streitz F H and Mintmire J W 1994 *Phys. Rev.* B **50** 11 996
[17] Landau L D and Lifshitz E M 1960 *Electrodynamics of Continuous Media* (Oxford: Pergamon)
[18] Parr R G and Yang Weitao 1989 *Density-Functional Theory of Atoms and Molecules* (New York: Oxford University Press)
[19] Zandbergen H W 1992 *Physica* C **194** 287
[20] Senet P, Lambin Ph, Vigneron J P, Derycke I and Lucas A 1991 *Surf. Sci.* **226** 307
[21] Jockisch A, Schröder U, de Wette F W and Kress W 1993 *J. Phys.: Condens. Matter* **5** 5401
[22] Litvinchuk A P, Thomsen C and Cardona M 1994 *Physical Properties of High Temperature Superconductors* vol 4, ed D M Ginsberg (Singapore: World Scientific) p 217